Energy Conversion and Management 153 (2017) 60–70

Contents lists available at ScienceDirect

Energy Conversion and Management

journal homepage: www.elsevier.com/locate/enconman

An improved modeling for low-grade organic Rankine cycle coupled with optimization design of radial-inflow turbine

Lijing Zhai[a], Guoqiang Xu[a], Jie Wen[a,*], Yongkai Quan[a], Jian Fu[a], Hongwei Wu[b,**], Tingting Li[c]

[a] National Key Laboratory of Science and Technology on Aero-Engine Aero-thermodynamics, School of Energy and Power Engineering, Beihang University, Beijing 100191, China

[b] School of Engineering and Technology, University of Hertfordshire, Hatfield AL10 9AB, United Kingdom

[c] Department of Mechanical Engineering, Texas A & M University, College Station, TX 77843-3123, United States

ARTICLE INFO

Keywords:
Organic Rankine cycle
Radial-inflow turbine
Coupled modeling
Genetic algorithm

ABSTRACT

Organic Rankine cycle (ORC) has been proven to be an effective and promising technology to convert low-grade heat energy into power, attracting rapidly growing interest in recent years. As the key component of the ORC system, turbine significantly influences the overall cycle performance and its efficiency also varies with different working fluids as well as in different operating conditions. However, turbine efficiency is generally assumed to be constant in the conventional cycle design. Aiming at this issue, this paper couples the ORC system design with the radial-inflow turbine design to investigate the thermodynamic performance of the ORC system and the aerodynamic characteristics of radial-inflow turbine simultaneously. The constrained genetic algorithm (GA) is used to optimize the radial-inflow turbine with attention to six design parameters, including degree of reaction, velocity ratio, loading coefficient, flow coefficient, ratio of wheel diameter, and rotational speed. The influence of heat source outlet temperature on the performance of the radial-inflow turbine and the ORC system with constant mass flow rate of the heat source and constant heat source inlet temperature is investigated for four kinds of working fluids. The net electrical powers achieved are from few tens kWs to one hundred kWs. The results show that the turbine efficiency decreases with increasing heat source outlet temperature and that the decreasing rate of turbine efficiency becomes faster in the high temperature region. The optimized turbine efficiency varies from 88.06% (using pentane at the outlet temperature of 105 °C) to 91.01% (using R245fa at the outlet temperature of 80 °C), which appears much higher compared to common values reported in the literature. Furthermore, the cycle efficiency increases monotonously with the growth of the heat source outlet temperature, whereas the net power output has the opposite trend. R123 achieves the maximum cycle efficiency of 12.21% at the heat source outlet temperature of 110 °C. Based on the optimized results, the recommended ranges of the key design parameters for ORC radial-inflow turbine are presented as well.

1. Introduction

Nowadays, with rapidly increasing globalization and energy demands, researchers are devoted to solving problems of energy shortage and environmental pollution. Apart from the development of new energy sources, the recovery and utilization of renewable energy, such as solar energy [1–3], biomass energy [4,5], geothermal energy [6–9] and waste heat [10–12], have attracted increasing attention. Because of the advantages of low capital cost, small size and easy maintenance [13], Organic Rankine cycle (ORC), which has the same configuration as conventional steam Rankine cycle but uses organic fluid instead of water as working fluid, has been proved to be an effective and promising technology for the low-grade heat recovery.

Over the past two decades, a large part of relevant research studies focuses on the working fluid selection. Dry and isentropic fluids with positive slopes or infinitely large slopes of vapor saturation curves in the temperature-entropy diagram are preferable due to their convenience in the non-superheating ORC [14]. Additionally, a suitable working fluid should also satisfy cycle and turbine performances, safety and environmental criteria [15]. Wang et al. [16] evaluated R11, R141b, R123, R245fa and R245ca as working fluids for engine waste heat recovery. R245fa and R245ca were recommended as the most suitable working fluids for an engine waste heat-recovery application. Rayegan and Tao [17] developed a procedure to compare 117 organic

* Corresponding author.
** Corresponding author.
E-mail addresses: wenjie@buaa.edu.cn (J. Wen), h.wu6@herts.ac.uk (H. Wu).

http://dx.doi.org/10.1016/j.enconman.2017.09.063
Received 26 June 2017; Received in revised form 18 September 2017; Accepted 23 September 2017

Nomenclature

Symbol

W	work/power, W
Q	heat, J
h	specific enthalpy, J/kg
Δh_{actual}	actual enthalpy drop, J/kg
Δh_s	isentropic enthalpy drop, J/kg
Δh	enthalpy difference, J/kg
T	temperature, K
P	pressure, Pa
ρ	density, kg/m^3
c	absolute velocity, m/s
w	relative velocity, m/s
u	peripheral velocity, m/s
m	mass flow rate, kg/m^3
r	radius, m
d	diameter, m
b	blade height, m
τ	blockage factor
h_c	tip clearance, m
E	energy, factor
H	form factor
C	loss coefficient multiplier, 1
l	surface length, m
s	blade spacing at blade-row exit, m
A	area, m^2
t	trailing-edge thickness, m
Z	blade number
Ma	Mach number
	diameter at the rotor shroud, m
$d_{2,h}$	diameter at the rotor hub, m
$d_{2,sh}$	mean diameter at the rotor outlet, m

Subscripts

wf	working fluid
0	nozzle inlet
1	nozzle outlet or rotor inlet
2	rotor outlet
cond	condenser
evap	evaporator
s	isentropic process
n	nozzle
r	rotor
m	meridional direction
u	peripheral direction
2-D	two dimensional
3-D	three dimensional
rel	relative
abs	absolute

Greek letters

η_{1st}	the first law efficiency of ORC system
$\eta_{turbine}$	turbine efficiency
α	absolute flow angle, degree
β	relative flow angle, degree
Ω	degree of reaction
φ	nozzle velocity coefficient
ψ	rotor velocity coefficient
Φ	flow coefficient
Ψ	loading coefficient
μ	dynamic viscosity, Pa·s
ξ	loss coefficient
ζ	energy loss coefficient
θ	momentum thickness, m
γ	flow angle, degree
ω	rotational speed, rpm

fluids in solar ORC. R245fa and R245ca were selected for the medium temperature level. Drescher and Bruggemann [18] investigated suitable working fluids for ORC in biomass power plants. It was found that the family of alkylbenzenes showed the highest cycle efficiencies. Qiu [19] proposed a preferable ranking of 8 mostly-applied working fluids by means of spinal point method in micro-CHP (combined heat and power) systems. In general, the selection of working fluids is a complex process, which is affected by the heat source type and level, operating conditions, cycle configuration, the turbine types and performance. The results of working fluid selection do not have universality because of widely varying cycle operation conditions, diverse cycle configurations, different aims for working fluid selection in terms of different application background and so forth [20].

It is also noted that determination and optimization of the ORC system parameters are another hot topic in the field of ORC. Peris et al. [21] studied the performance of a regenerative ORC with heat source inlet temperature of 127–156 °C experimentally. The inlet pressure of volumetric expander was about 14–20 bar and the maximum electrical efficiency of 12.32% was obtained at the heat source inlet temperature of 155 °C. Braimakis and Karellas [22] presented an integrated thermoeconomic optimization approach of standard and regenerative ORCs. It was concluded that for small scale ORCs the most important costs were related to heat exchangers and the pump while for large scale ORCs screw expanders and turbines were preferred and they had very high costs. Mehrpooya and Ashouri [23] performed a thermoeconomic analysis of a regenerative two-stage ORC with solar energy as heat source to minimize the product cost and maximize the exergy efficiency. The cycle efficiency of 19.59% was reached and product cost rate was 3.88 million dollars per year. Yang and Yeh [24] analyzed the ORC system for geothermal application with heat source inlet temperature of 100 °C and mass flow rate of 80 kg/s and found that the higher the operating pressures were, the larger the proportion of purchased cost would be. Marion et al. [25] conducted theoretical and experimental studies on a solar subcritical ORC and concluded that the net mechanical power strongly depended on the fluid mass flow rate and that the optimum mass flow rate was a linear function of the solar radiation. Apart from the standard ORC system, advanced ORC systems like recuperative ORC [26,27], regenerative ORC [22,28], supercritical ORC [29–31], zeotropic ORC [32,33] and trilateral cycle [34,35] also have been studied extensively.

The turbine design is a critical step in the design of ORC systems since turbine geometry and aerodynamic performance directly affect the overall cycle performance and vice versa. Among kinds of ORC expanders, the radial-inflow turbine shows good aerodynamic performance due to its capability of dealing with large enthalpy drops with relatively low peripheral speeds [36]. The conventional turbine design method used for gas turbine is also applicable to the design of an ORC turbine. Due to the lack of extensive experimental data, the loss models are often based on the experimental studies of gas turbine. Fiaschi et al. [36] discussed a 0-D model for the design of radial turbine for 50 kW ORC applications and investigated the estimation of the turbine losses and the main design parameters. The total-to-total efficiency of the designed turbine ranged from 0.72 to 0.80 and backswept bladed rotors showed 1.5–2.5% higher efficiencies. Song et al. [37] proposed a 1-D aerodynamic analysis model of the radial-inflow turbine and a performance prediction model of the heat exchanger. The expansion ratio of

the six working fluids in the radial-inflow turbine was about 5–25 when the evaporation temperature was 360–430 K. Sauret and Gu [38] performed preliminary steady-state 3-D computational fluid dynamics (CFD) simulations of radial turbine for a number of operating conditions. The maximum turbine efficiency was 88.45% with rotational speed of 25463.5 rpm and turbine inlet temperature of 413 K. Kang [39] examined a two-stage radial turbine with the expansion ratio of the high-pressure turbine as 2.67 and the expansion ratio of the low-pressure turbine as 4.07. The maximum electric power, average cycle and turbine efficiencies were found to be 39.0 kW, 9.8% and 58.4% when the evaporation temperature was 116 °C. When it comes to the optimization design of fluid machinery, the genetic algorithm (GA), simulated annealing algorithm, particle swarm optimization (PSO) and ant colony optimization (ACO) are frequently used. Since the GA can deal with complex optimization problems and is less sensitive to the initial conditions, it is distinguished from other optimization methods with respect to the optimization design of turbines for ORC systems, and is the most widely used method to select parameters about the turbine size [13], stage geometry [15,40] and turbine performance.

In the conventional design of the ORC system, the turbine efficiency is a fixed value. But in practical application, the turbine efficiency is directly related with the selected working fluids and the system operating conditions. At the same time, the system parameter determination is also influenced by the turbine performance. It's necessary to couple the modeling of ORC system with the preliminary design of radial-inflow turbine. Song et al. [41] presented a 1-D analysis model of the radial-inflow turbine in the ORC system design with seven key parameters determining the turbine geometry and aerodynamic performance as fixed values. Pan and Wang [42] replaced the constant isentropic efficiency with the internal efficiency of optimal radial turbine for each condition and analyzed the effects of evaporating temperature on cycle performance. This study focused on the optimization of degree of reaction, hub-diameter ratio and peripheral velocity ratio while remaining other parameters constant. Jubori et al. [43] presented an integrated approach combining ORC system modeling, mean-line design and 3-D CFD analysis for micro-scale axial and radial-inflow turbines with the maximum total-to-total efficiency as 83.48% and 83.85%, respectively. It appears from the previous investigations that the existing research aforementioned mainly focused on the study of ORC system or radial turbine only. To the best of the authors' knowledge, however, the exploration of the coupled design of the ORC system and its radial-inflow turbine has been far from complete and there is still much room to be enhanced in this area. Moreover, the recommended values of the key design parameters for the ORC radial-inflow turbine are not extensively studied.

In this paper, an ORC model is built for the utilization of geothermal resource with heat source inlet temperature of 120 °C. A coupled design of the ORC system and the radial-inflow turbine is performed with the constrained GA to maximize the turbine efficiency. The ORC systems with different heat source outlet temperatures and working fluids are investigated by an original MATLAB code. The analysis of the optimized parameters: degree of reaction, velocity ratio, loading coefficient, flow coefficient, ratio of wheel diameter and rotational speed, is conducted. In addition, this paper also provides references on the recommended ranges of the key design parameters for ORC radial-inflow turbine based on the optimized results.

2. ORC modeling and working fluid candidates

2.1. ORC modeling

Fig. 1 shows the schematic diagram of a basic ORC system, which includes four main components: working fluid pump, evaporator, turbine and condenser. The temperature-entropy diagram of the basic ORC using pentane is shown in Fig. 2.

The work consumed by the pump in the process 3–4 is expressed by:

$$W_{pump} = m_{wf}(h_4 - h_3) = m_{wf}(h_{4s} - h_3)/\eta_{pump} \quad (1)$$

The heat absorbed in the evaporator in the process 4 to 0 is expressed by:

$$Q_{evap} = m_{wf}(h_0 - h_4) = m_{evap}(h_{evap,in} - h_{evap,out}) \quad (2)$$

The work produced by the turbine in the process 0 to 2 is expressed by:

$$W_{turb} = m_{wf}(h_0 - h_2) = m_{wf}(h_0 - h_{2s}) \cdot \eta_{turbine} \quad (3)$$

The heat generated in the condenser in the process 2 to 3 is expressed by:

$$Q_{cond} = m_{wf}(h_2 - h_3) = m_{cond}(h_{cond,out} - h_{cond,in}) \quad (4)$$

The net power output of the ORC system is expressed by:

$$W_{net} = W_{turbine} - W_{pump} \quad (5)$$

The first law efficiency of the ORC system can be calculated by:

$$\eta_{1st} = \frac{W_{net}}{Q_{evap}} = \frac{W_{turbine} - W_{pump}}{Q_{evap}} = \frac{(h_0 - h_2) - (h_4 - h_3)}{h_0 - h_4} \quad (6)$$

The conditions for the heat source, heat sink and ORC system are summarized in Table 1. The working conditions are applied to the utilization of geothermal resource with fixed heat source temperature and mass flow rate.

2.2. Working fluid candidates

Working fluid plays an important role in the design and performance analysis of an ORC system. It not only affects the turbine aerodynamic performance but also its geometry. Generally, the organic working fluids are divided into three categories: wet, dry and isentropic in terms of the slope of the saturated vapor line in the T-s diagram. Due to the low temperature of the heat source, this study selects four commonly used dry working fluids, pentane, R245fa, R365mfc and R123 [13,36,44]. This ensures that there are no liquid working fluids existing in the rotor and thus there is no need to superheat the working fluids. Table 2 shows the properties of the selected working fluid candidates.

3. Turbine design

The preliminary design of the radial turbine is performed by the mean-line approach, which is on the basis of a one-dimensional assumption that there is a mean streamline through the stage [13]. Conservation of mass, momentum and energy together with velocity triangle equation, state equation and loss model are used to determine the parameters of basic geometry, velocity triangles, thermodynamic properties. In this paper, volute and expansion diffuser are ignored in order to simplify computational load. The simplified working procedure is shown in Fig. 3, where point 0 represents the state of the working fluid at the nozzle inlet, point 1 represents the state at the nozzle outlet as well as the state at the rotor inlet, and point 2 represents the state at the rotor outlet. $\Delta h_s$is the isentropic enthalpy drop of the entire turbine

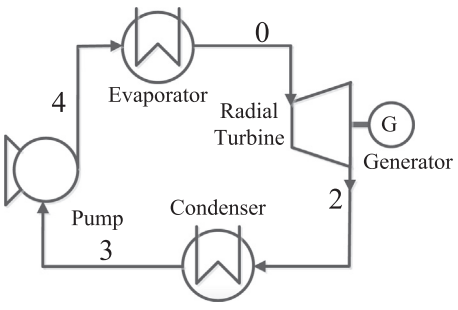

Fig. 1. Schematic diagram of the basic ORC.

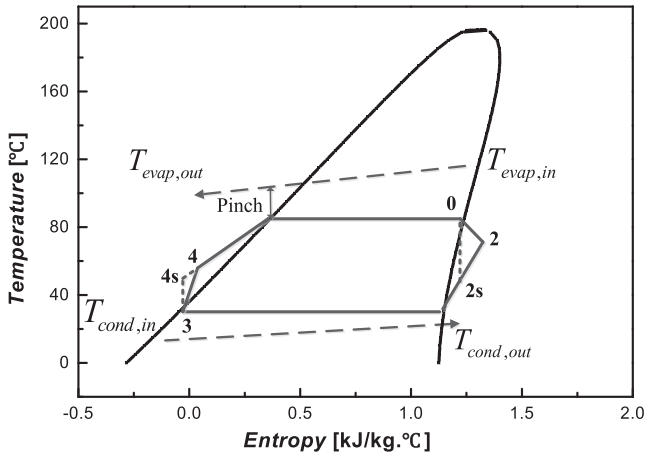

Fig. 2. Temperature-entropy curve of the basic ORC (using pentane).

Table 1
Working conditions for the heat source, heat sink and cycle parameters.

System	Parameters	Value
Heat source (water)	Inlet temperature (°C)	120
	Pressure (kPa)	500
	Mass flow rate (kg/s)	10
Heat sink (water)	Inlet temperature (°C)	25
	Outlet temperature (°C)	35
	Pressure (kPa)	250
ORC	Isentropic pump efficiency	0.8
	Pinch temperature in the evaporator (°C)	12
	Pinch temperature in the condenser (°C)	8

Table 2
Properties of the working fluid candidates.

Fluid	Molecular weight (g/mol)	Critical pressure (kPa)	Critical temperature (°C)	Normal boiling point (°C)	GWP (100 yr)	ODP
Pentane	72.15	3370	196.55	36.06	20	0
R245fa	134.05	3651	154.01	15.14	950	0
R365mfc	148.07	3266	186.85	40.15	794–997	0
R123	152.93	3662	183.68	27.82	77	0.02

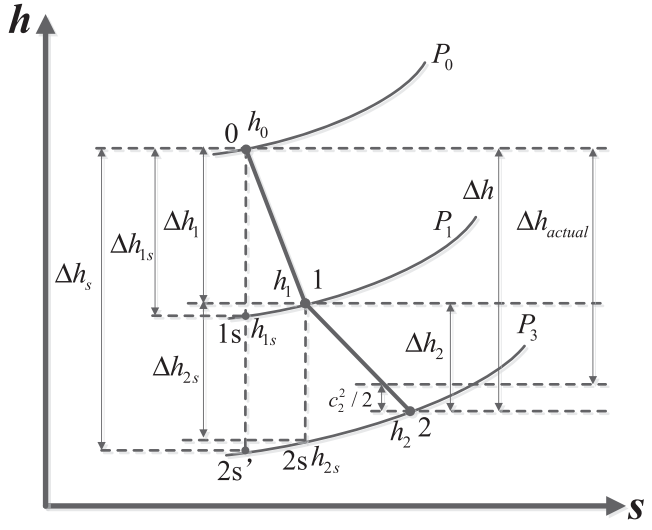

Fig. 3. *h-s* diagram of the radial-flow turbine.

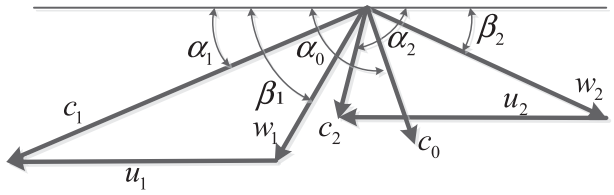

Fig. 4. Velocity triangles of the radial-inflow turbine.

and Δh_{actual} is the actually useful enthalpy drop which does not account for the energy of leaving velocity.

Absolute velocity, relative velocity and velocity angles at the nozzle outlet and rotor outlet are determined according to velocity triangles of the radial-inflow turbine as shown in Fig. 4.

As shown in Fig. 3, working fluid flows through the nozzle and rotor. From state point 0 to state point 1, the flow equations of the working fluid can be expressed as follows, where the subscripts 0, 1 and 2 represent the same state point in Fig. 3:

Mass continuity equation: $m_{wf} = \rho_1 c_{1m} b_{1n} d_{1n} \pi \tau_n$ (7)

Energy equation: $\begin{cases} \Delta h_{1s} = (1-\Omega)\cdot\Delta h_s, h_{1s} = h_0 - \Delta h_{1s} \\ h_1 = h_{1s} + (c_{1s}^2 - c_1^2)/2 = h_{1s} + c_{1s}^2(1-\varphi^2)/2, \quad c_1 = \varphi c_{1s} \end{cases}$ (8)

Equation of state: $P_1 = f(h_{1s}, s_0), T_1 = f(P_1, h_1), \rho_1 = f(P_1, h_1)$ (9)

Velocity triangle: $u_1 = (u_1/c_s)\cdot c_s, \quad c_{1m} = \Phi\cdot u_1, \quad c_{1u} = \sqrt{c_1^2 - c_{1m}^2}$ (10)

where τ_n is the nozzle blockage factor. c_s $(=\sqrt{2\Delta h_s})$ is the ideal velocity of the working fluid at the turbine outlet. c_{1m} and c_{1u} are the absolute velocity in the meridional and peripheral directions at the nozzle outlet, respectively. φ is the nozzle velocity coefficient. u_1/c_s is the velocity ratio. Φ is the flow coefficient ($\Phi = c_{1m}/u_1$). Ω is the degree of reaction. b_{1n} is the nozzle blade height and d_{1n} is the nozzle outlet diameter.

From state point 1 to state point 2, the flow equations of the working fluid can be expressed as follows:

Mass continuity equation: $m_{wf} = \rho_1 c_{1m} b_1 d_1 \pi \tau_1 = \rho_2 c_{2m} b_2 \pi \cdot (d_{2,s} + d_{2,h})/2 \cdot \tau_2$ (11)

Energy equation: $\begin{cases} h_2 = h_{2s} + (w_{2s}^2 - w_2^2)/2 + L_{df} + L_c \\ = h_{2s} + w_{2s}^2(1-\psi^2)/2 + L_{df} + L_c, \quad w_2 = \psi w_{2s} \end{cases}$ (12)

Equation of state: $T_2 = f(P_2, h_2), \rho_2 = f(T_2, h_2)$ (13)

Velocity triangle: $u_2 = \mu u_1, c_{2u} = (c_1\cdot cos\alpha_1\cdot u_1 - u_1^2\cdot\Psi)/u_2, \quad c_{2m} = \sqrt{c_2^2 - c_{2u}^2}$ (14)

where τ_1 and τ_2 are the rotor inlet and outlet blockage factors, respectively. c_{2m} and c_{2u} are the absolute velocity in the meridional and peripheral directions at the rotor outlet, respectively. ψ is the rotor velocity coefficient. μ is the ratio of wheel diameter ($\mu = d_{2,sh}/d_1$). Ψ is the load coefficient ($\Psi = (u_1 c_{1u} - u_2 c_{2u})/u_1^2$). b_1 is the nozzle blade height and d_1 is the nozzle outlet diameter. $d_{2,s}$ and $d_{2,h}$ are the diameter at the rotor shroud and hub, respectively. L_{df} and L_c are the disk-friction loss and tip clearance loss, respectively.

Five kinds of turbine loss are taken into consideration in the preliminary design, including the nozzle passage loss, rotor passage loss, leaving velocity loss, disk-friction loss and tip clearance loss. The nozzle passage loss coefficient (ξ_n), rotor passage loss coefficient (ξ_r) and leaving velocity loss coefficient (ξ_e) are expressed as follows:

$\xi_n = (1-\varphi^2)(1-\Omega)$ (15)

$\xi_r = (w_2/c_s)^2(1/\psi^2 - 1)$ (16)

$\xi_e = (c_2/c_s)^2$ (17)

Disk-friction loss (L_{df}) and coefficient (ξ_{df}), tip clearance loss (ξ_c) and coefficient (L_c) are expressed as follows [45]:

$$\xi_{df} = \frac{0.02125\rho_1 u_1^3 r_1^2}{\left(\frac{\rho u r}{\mu}\right)_1^{0.2} \cdot m_{wf} \cdot \Delta h_s} \tag{18}$$

$$L_{df} = \xi_{df} \cdot \Delta h_s \tag{19}$$

$$\xi_c = \frac{h_c}{r_{2,s} - r_{2,h}} \tag{20}$$

$$L_c = \xi_c \cdot \Delta h_s \tag{21}$$

where h_c is the tip clearance, specified as 0.3 mm. This loss model assumes that the fractional loss due to tip clearance equals to the ratio of clearance to passage height at the rotor exit.

Turbine efficiency (total to static efficiency) is expressed as:

$$\eta_{turbine} = \frac{\Delta h_{actual}}{\Delta h_s} = \frac{\Delta h - c_2^2/2}{\Delta h_s} \tag{22}$$

The power output is calculated as follows:

$$W = \Delta h_{actual} m_{wf} \eta_{turbine} \tag{23}$$

4. Coupled model of ORC and radial-inflow turbine with genetic algorithm

4.1. Velocity coefficient

According to Eqs. (7)–(14), nozzle velocity coefficient (φ), rotor velocity coefficient (ψ), degree of reaction (Ω), velocity ratio (u_1/c_s), loading coefficient (Ψ), flow coefficient (Φ), ratio of wheel diameter (μ) are seven key dimensionless parameters when designing the radial-inflow turbine. In the preliminary design of conventional turbine, φ and ψ are estimated and specified according to the empirical formula since they are dependent on many factors, such as the blade profile, machining precision, fluid flow conditions and so forth. This study uses the loss models proposed by the Lewis Research Center [45] to calculate these two parameters iteratively. The relationships of φ and ψ with nozzle and rotor energy loss coefficients (ζ_n and ζ_r) are as follows:

$$\varphi = \sqrt{1-\zeta_n}, \quad \psi = \sqrt{1-\zeta_r} \tag{24}$$

ζ_n and ζ_r can be expressed in a unified formula:

$$\zeta_{3D} = \frac{EC\left(\frac{\theta_{tot}}{l}\right)_{ref}\left(\frac{Re}{Re_{ref}}\right)^{-0.2}\left(\frac{l}{s}\right)\left(\frac{A_{3D}}{A_{2D}}\right)}{\cos\gamma - \frac{t}{s} - HC\left(\frac{\theta_{tot}}{l}\right)_{ref}\left(\frac{Re}{Re_{ref}}\right)^{-0.2}\left(\frac{l}{s}\right)} \tag{25}$$

where E is the energy factor and H is the form factor, which presents the characteristics of boundary layer flow and can be calculated by empirical equations. C is the loss coefficient multiplier. Re is the Reynolds number. θ is the momentum thickness. l is the surface length from leading edge to trailing edge. s is blade spacing at blade-row exit. A_{3D}/A_{2D} represents the 3-D to 2-D area ratio. γ is the flow angle from the throughflow direction. t is the trailing-edge thickness. All these related factors are discussed in detail in [45] and can be calculated according to the corresponding formulas. Some parameters need to be known in advance in order to complete the preliminary design of the radial-inflow turbine and obtain some parameters related to the geometry: the tip clearance value is fixed as 0.3 mm considering the manufacture technology; the radial clearance between nozzle and rotor is specified as 1 mm [46]; the nozzle solidity is specified as 1.3 according to [47]. Nozzle blade uses the TC-4P blade profile which is a commonly used stator profile in the ORC system and thus the nozzle inlet absolute flow angle α_0 can be obtained. Initial φ and ψ are presupposed in advance to finish the preliminary design of the radial-inflow turbine. Then ζ_n and ζ_r can be calculated by Eq. (25), after which φ and ψ are updated by Eq. (24) to proceed to the next iteration until the differences in velocity coefficients of two iteration are within a minimum range.

Table 3
Recommended value ranges of the six optimized variables.

Design variables	Range	Reference
Degree of reaction (Ω)	0.50–0.60	[48]
Velocity ratio (u_1/c_s)	0.69–0.71	[36]
Loading coefficient (Ψ)	0.85–1.00	[38]
Flow coefficient (Φ)	0.15–0.30	[38]
Ratio of wheel diameter (μ)	0.50–0.60	[46]
Rotational speed (ω, rpm)	12,000–25,000	[38]

4.2. Optimization method

In addition to the other five dimensionless parameters (Ω, u_1/c_s, Ψ, Φ, μ), rotational speed (ω) should also be optimized since its optimal value varies with operating conditions. In this work, turbine efficiency is specified as the objective function to optimize the radial-inflow turbine for each operating condition since under this condition the optimized results of the power output as the optimization objective are very similar to that of the turbine efficiency as the optimization objective.

The six optimized variables are limited by empirical values, as listed in Table 3.

Some optimization constraints are implemented in this model to ensure the reasonable results of optimized turbine in terms of high aerodynamic performance and ease of manufacture.

- The nozzle outlet absolute blade angle α_1 is recommended between 12 and 30° and the rotor outlet relative blade angle β_2 is recommended between 20 and 45° [46]. These values are established with the trade-off between the high stage shaft power and low flow losses.
- The ratio of the rotor inlet blade height and diameter is considered to lie between 0.03 and 0.1 [46]. This value is set to limit the rotor tip clearance losses.
- The nozzle outlet Mach number is limited less than 1.5 to lower the supersonic loss at the rotor inlet.
- The hub ratio (rotor exit hub to inlet radius ratio, $d_{2,h}/d_1$) is set more than 0.2 since the smaller hub ratio leads to great difficulty in assigning blades at the hub [44].

In this work, the genetic algorithm (GA) is used to complete the optimization of the six key design parameters. The GA is a global optimum algorithm based on the theory of biological evolution [49]. Compared with other optimization methods, the GA has many advantages. It can not only deal with complex optimization problems such as non-linear and multi-dimensional but also is less sensitive to the initial conditions. Therefore, the GA is widely used in many literatures about ORC systems [13,15,40]. In the basic GA, the initial population of individuals is generated randomly from the prescribed range of optimization variables. All individuals in every generation are assessed in terms of their fitness values. A new generation of individuals is generated by selecting the current population according to their fitness values, crossovering the selected members according to the crossover rate and mutating certain individuals according to the mutation rate. Therefore, selection, crossover and mutation are the three main operations in GA. The flowchart of the constrained GA is shown in Fig. 5. The control operators of GA are listed in Table 4.

4.3. Simulation method

Fig. 6 shows the flowchart of the simulation process of the ORC

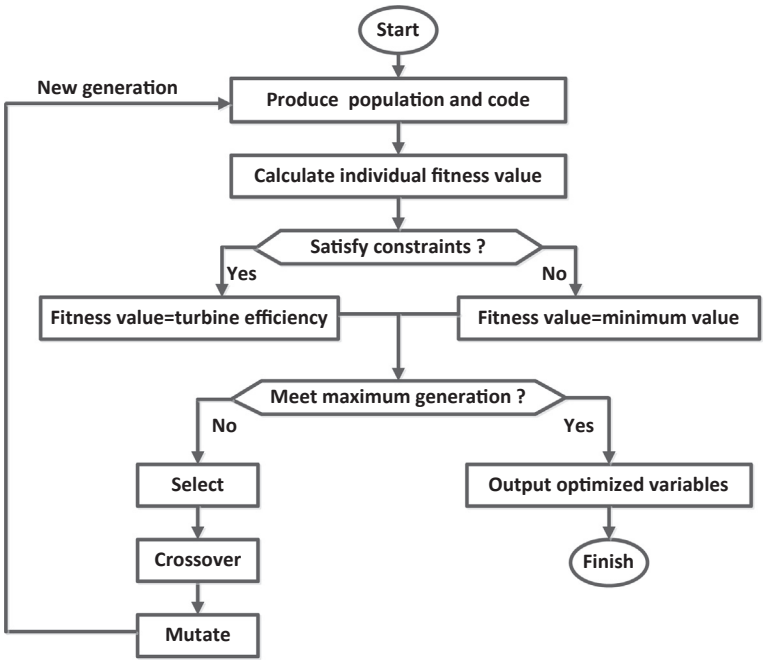

Fig. 5. Flowchart of the constrained GA.

Table 4
Control operators of GA.

Operator	Value
Maximum number of generations	200
Number of individuals	80
Selection rate	0.9
Crossover probability	0.7
Mutation rate	0.01

system, in which the optimization design of the radial-inflow turbine with constrained GA is introduced. The pinch methodology is used here to simulate the ORC cycle. To simplify the ORC modeling, the turbine inlet and condenser outlet are assumed to be saturated vapor state and saturated liquid state, respectively. The turbine efficiency is varying with the operation conditions of the ORC system instead of being constant in the conventional ORC system design. Three initial input parameters, turbine inlet temperature (T_0), condenser outlet temperature (T_3), and turbine efficiency ($\eta_{turbine}$) are estimated as the initial input data to start the simulation. In the preliminary optimization design, constrained GA optimizes six key parameters in the experience value range as listed in Table 4, and the iterative solving process determines the velocity coefficients of nozzle and rotor. After each loop, the newly obtained values of the turbine inlet and outlet temperature as well as the condenser outlet temperature are updated. If the requirements of the three parameters are not reached as shown in Fig. 6, they are used again as the initial input data to continue the next loop. However, initially turbine efficiency is estimated instead of the turbine outlet temperature. This is because at the beginning it is difficult to estimate the turbine outlet temperature while turbine efficiency can be estimated by experience. The process is repeated until the requirements of the turbine outlet temperature, the pinch temperature in the evaporation and condenser are met. Pinch point in the evaporation appears at the saturated liquid state of the working fluids and pinch point in the condenser appears at the saturated vapor state of the working fluids. An original MATLAB code is programmed to simulate the described ORC system and optimization design of radial-inflow turbine. The properties of working fluids are obtained from REFPROP 9.0 [50]. The simulation is assumed to operate at the steady state and to neglect the pressure and heat losses in the entire cycle.

5. Results and discussion

5.1. Validation of the turbine design model

The turbine design model described in Section 3 is validated by the comparison of the developed codes with other published codes: Glassman [45], commercial radial turbine design software RITAL from Concepts NREC [51] and Rahbar et al. [52]. The testing conditions are from Glassman case [45] and the results of different codes are shown in Table 5. The set of results from the developed model in this work shows a good agreement with both the original one and literature in terms of flow characteristic, turbine principal geometry and overall performance. It should be noticed that the turbine total-to-static efficiency predicted by the developed code in this work is closer to the original efficiency than the other two kinds of codes. Therefore, the turbine design model is considered to be validated for the coupled modeling of ORC system and its radial-inflow turbine.

5.2. Optimization results

The turbine design model validated in Section 5.1 is used to study the coupled modeling of ORC system and its radial-inflow turbine, and to investigate the influence of heat source temperature. The overall examined range of the heat source outlet temperature is set from 110 °C to 80 °C. For pentane and R245fa the temperature range is 80–105 °C while for R365mfc and R123 the temperature range is 90–110 °C. Out of these ranges, certain design parameters of the radial-inflow turbine cannot satisfy the constraints proposed in Section 4 and thus there is no data at this point. The variations of pressure ratio and mass flow rate with the outlet temperature of the heat source are first shown in Fig. 7.

Under the condition of fixed mass flow rate for the heat source, as the outlet temperature of the heat source decreases, more heat load is absorbed by the ORC system and thus the mass flow rate of the working fluids increases. The cycle using R123 has the highest mass flow rate at any conditions while using pentane has the lowest mass flow rate. The lower outlet temperature of the heat source causes the evaporation temperature to decrease and thus to lower the pressure ratio. R365mfc has the highest pressure ratio at each condition while for pentane, R245fa and R123 the pressure ratios are similar.

The turbine efficiency depending on different working fluids and

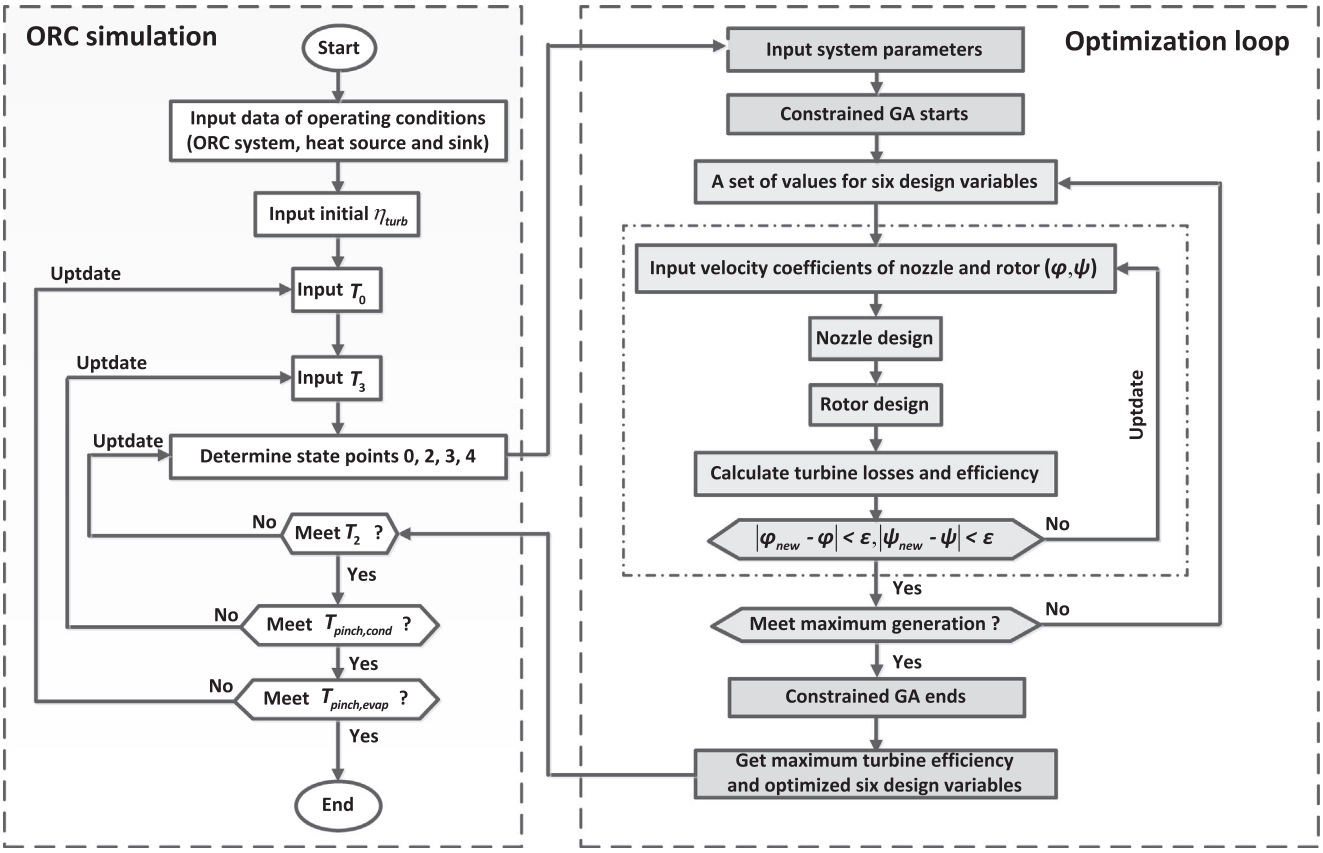

Fig. 6. Flowchart of the coupled ORC-turbine model.

Table 5
Comparison of developed code with published codes.

Parameter	Glassman [45]	RITAL [51]	Rahbar et al. [52]	Present code
Stator				
Inlet radius, m	0.09775	0.1033	0.09911	–
Outlet radius, m	0.07983	0.08268	0.08133	0.07795
Outlet absolute flow angle, deg.	18	26.61	21.89	18.09
Rotor				
Inlet radius, m	0.0777	0.07874	0.07888	0.07695
Outlet hub radius, m	0.01936	0.02362	0.02312	0.01995
Outlet shroud radius, m	0.05542	0.05591	0.05546	0.0546
Inlet absolute flow angle, deg.	18.08	26.87	26.49	18.09
Inlet relative flow angle, deg.	121.5	116.27	116.64	123.55
Outlet absolute flow angle, deg.	90	90.01	90	90.56
Outlet relative flow angle, deg.	35.10	34.42	36.24	35.1399
Total-to-static efficiency, %	82	79	78.8	79.45
Power, kW	22.371	–	–	21.52

heat source temperature conditions are shown in Fig. 8. The optimized turbine efficiency varies from 88.06% using pentane at the heat source outlet temperature of 105 °C to 91.01% using R245fa at the heat source outlet temperature of 80 °C. Fig. 8 also shows that the turbine efficiency decreases with the increase of the heat source outlet temperature. This indicates that smaller pressure ratio and larger mass flow rate enhance the turbine efficiency. In addition, the decreasing rate of turbine efficiency becomes faster when the heat source outlet temperature is greater than 100 °C, especially for pentane and R245fa. R123 and R365mfc also have this similar trend but the decreasing rate is respectively less intense. This can be explained by the loss distribution shown in Fig. 9, which illustrates the variations of five kinds of losses related with the heat source outlet temperature using pentane and R123 as working fluids. Fig. 9 shows that the rotor passage loss has the highest contribution for all the examined working fluids. As the outlet temperature of the heat source increases, the rotor passage loss increases gradually, especially violently when the heat source outlet temperature is greater than 100 °C. For pentane and R245fa, when the heat source outlet temperature increases from 100 °C to 105 °C, the increasing rate of the rotor passage loss coefficient is 20.92% and 17.05%, respectively. While for R365mfc and R123 the change rate is within 4.5%. This great increase of the rotor passage loss accounts for the sudden drop of the turbine efficiency using pentane and R245fa. Since the pressure ratio increases with the higher outlet temperature of the heat source, the velocity at rotor becomes larger leading to higher rotor passage loss. In addition, the loss distribution is similar for all the examined working fluids with the rotor passage loss having the highest contribution, varying from 32.15% to 37.40% of the total losses. The nozzle passage loss, rotor passage loss and leaving velocity loss are diverse in the same order of magnitude. Disk-friction loss and tip clearance loss are one magnitude lower than the above three kinds of losses. As shown in Fig. 9, both the disk-friction loss and tip clearance loss increase with the rise of the heat source outlet temperature. This is consistent with the conclusion that high expansion ratio leads to high friction loss [42].

The simulated results of the cycle efficiency, net power output and specific net power per mass flow rate are successively plotted in Figs. 10–12. Fig. 10 shows the cycle efficiency increases with the rise of the heat source outlet temperature while the net power has the opposite trend. This is due to the fact that the mass flow rate of the working fluids increases and enthalpy drop decreases with the lower heat source

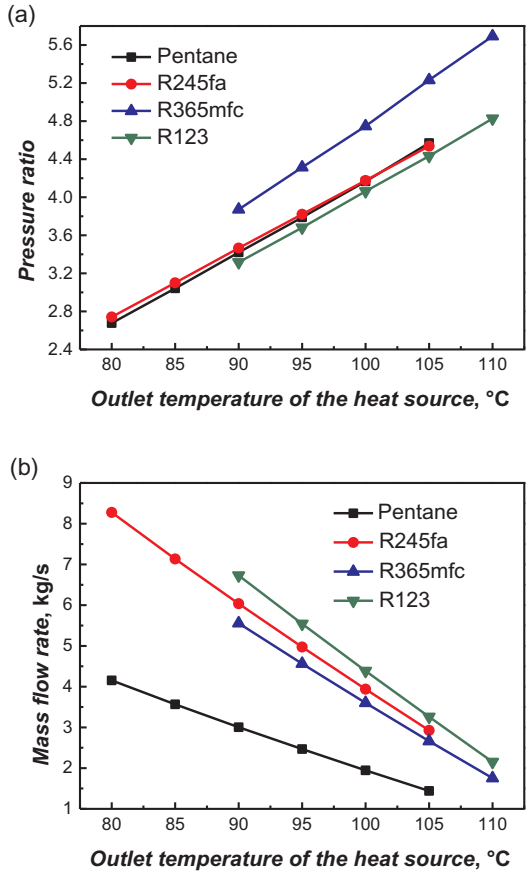

Fig. 7. Variations of (a) pressure ratio and (b) mass flow rate with the outlet temperature of the heat source.

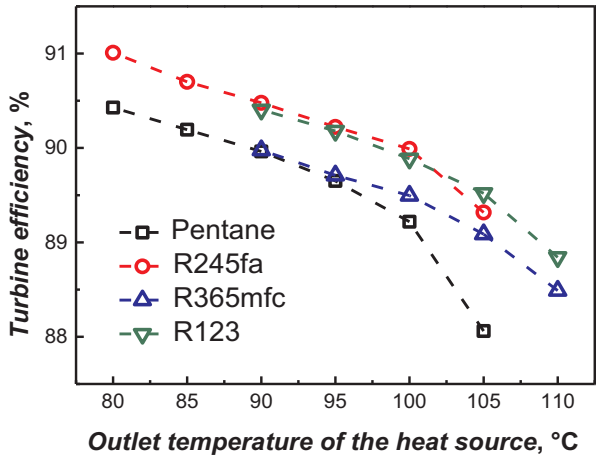

Fig. 8. Variation of turbine efficiency with the outlet temperature of the heat source.

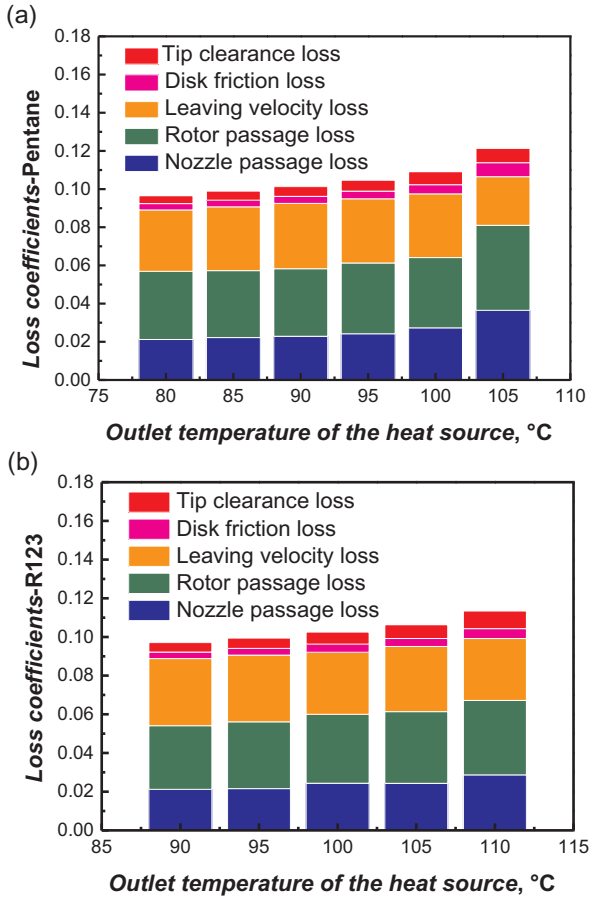

Fig. 9. Variations of the five kinds of losses with the outlet temperature of the heat source using pentane and R123.

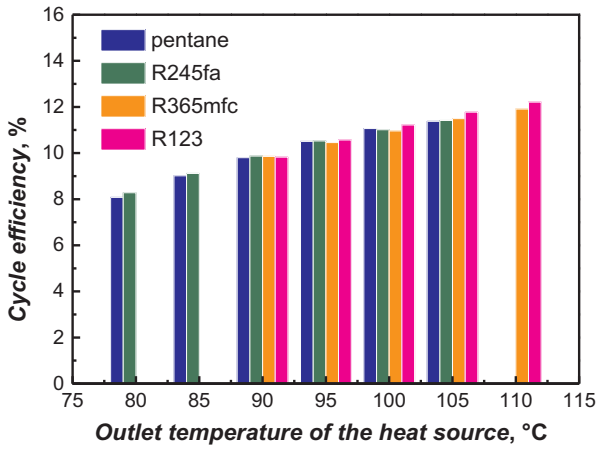

Fig. 10. Variation of cycle efficiency with the outlet temperature of the heat source.

outlet temperature, but the increase degree of the mass flow rate is much larger than the decrease degree of the enthalpy drop, which accounts for the increase of the net power. Take R123 for example, the enthalpy drop is −23.23% while the increase of the mass flow rate is 212.60% when the outlet temperature of the heat source changes from 110 °C to 90 °C. Moreover, it can be noticed that the differences of both the cycle efficiency and the net power output among different working fluids at each condition are not substantial. As shown in Fig. 12, the specific net power per mass flow rate increases with the higher heat source outlet temperature. Though the turbine efficiency using pentane is the lowest at each condition presented in Fig. 8, the specific net power is much higher than the other three kinds of working fluids. This indicates that pentane has the highest enthalpy drop among the examined working fluids. In the situation where the inlet temperature of the heat source rather than the absorbed heat load is fixed, the ORC cycle efficiency and the net power output change monotonously with the heat source outlet temperature, but their variation trends are in the opposite direction. From the perspective that the net power output is the main aim of the ORC system, the lower the outlet temperature of the heat source is, the better. Among the four examined working fluids, R123 achieves the maximum cycle efficiency of 12.21% together with the turbine efficiency of 88.84% at the heat source outlet temperature of 110 °C. R245fa achieves both the maximum net power output of

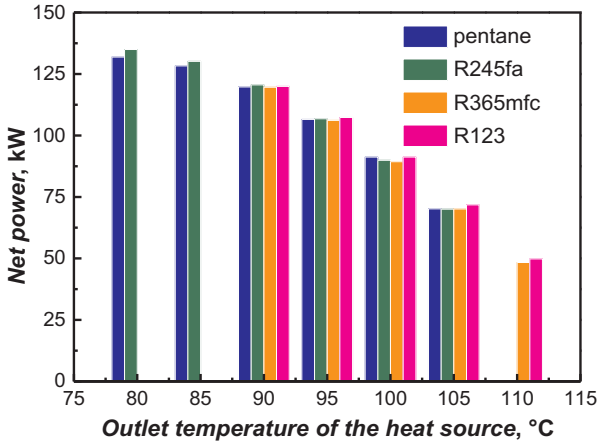

Fig. 11. Variation of net power with the outlet temperature of the heat source.

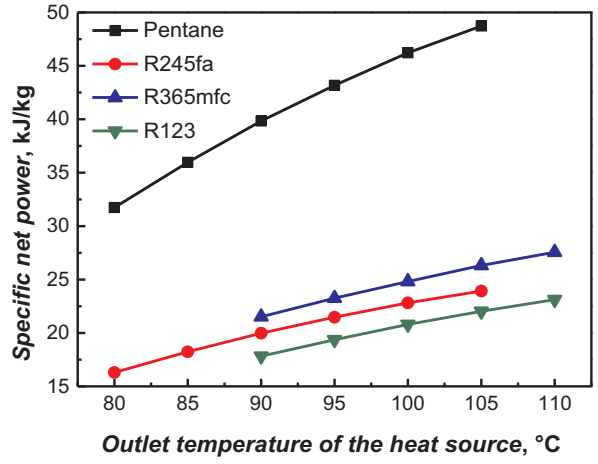

Fig. 12. Variation of specific net power with the outlet temperature of the heat source.

138.74 kW and the maximum turbine efficiency of 91.01% at the heat source outlet temperature of 80 °C.

In the following section a thorough analysis of the optimized results of the six key design parameters is conducted to provide references for ORC radial-inflow turbine in the low temperature range. Fig. 13 shows the optimized results of rotational speed, overall diameter (d_0) and Mach number at the rotor inlet with the outlet temperature of the heat source.

As shown in Fig. 13, the rotational speed increases with the rise of the heat source outlet temperature. Since the enthalpy drop increases with the higher heat source outlet temperature, higher rotational speed is required to provide the larger peripheral speed and more wheel periphery work. Taking R245fa for example, the rotational speed increases from 12,114 rpm to 24,959 rpm when the heat source outlet temperature changes from 80 °C to 90 °C, which amounts to 106.03% growth rate. In addition, pentane has the highest rotational speed at each condition. This is expected because pentane has the largest enthalpy drop among the examined fluids discussed previously. Fig. 13 also indicates that pentane reaches its rotational speed constraint when the heat source outlet temperature is more than 100 °C.

Considering the practicability of manufacture, some parameters related to the turbine geometry, including the hub ratio ($d_{2,h}/d_1$), the inlet diameter of the turbine (d_0) and the ratio of the rotor inlet blade height and diameter (b_1/d_1), restrict the upper and lower limits of the heat source outlet temperature. For the examined working fluids, as the outlet temperature of the heat source increases, the inlet diameter of the turbine decreases because of the reduction in the mass flow rate of the working fluids. The minimum overall diameter $d_0$is achieved by R245fa at the heat source outlet temperature of 105 °C (d_0 = 167.2 mm) while the largest size is achieved by pentane at the heat source outlet temperature of 80 °C (d_0 = 341.4 mm). The rotor exit hub to inlet radius ratio is in the range of 0.2017–0.2785 and is consistent with the literature [15,44]. Fig. 13 shows the variation of Mach number at the rotor inlet ($Ma_{1,abs}$) with the outlet temperature of the heat source. $Ma_{1,abs}$ increases with the higher heat source outlet temperature and R365mfc has the highest $Ma_{1,abs}$ at all conditions because of combined effect of the high peripheral speed and low density while R123 has the lowest. Except the condition of heat source outlet temperature of 80 °C, all the examined working fluids have supersonic

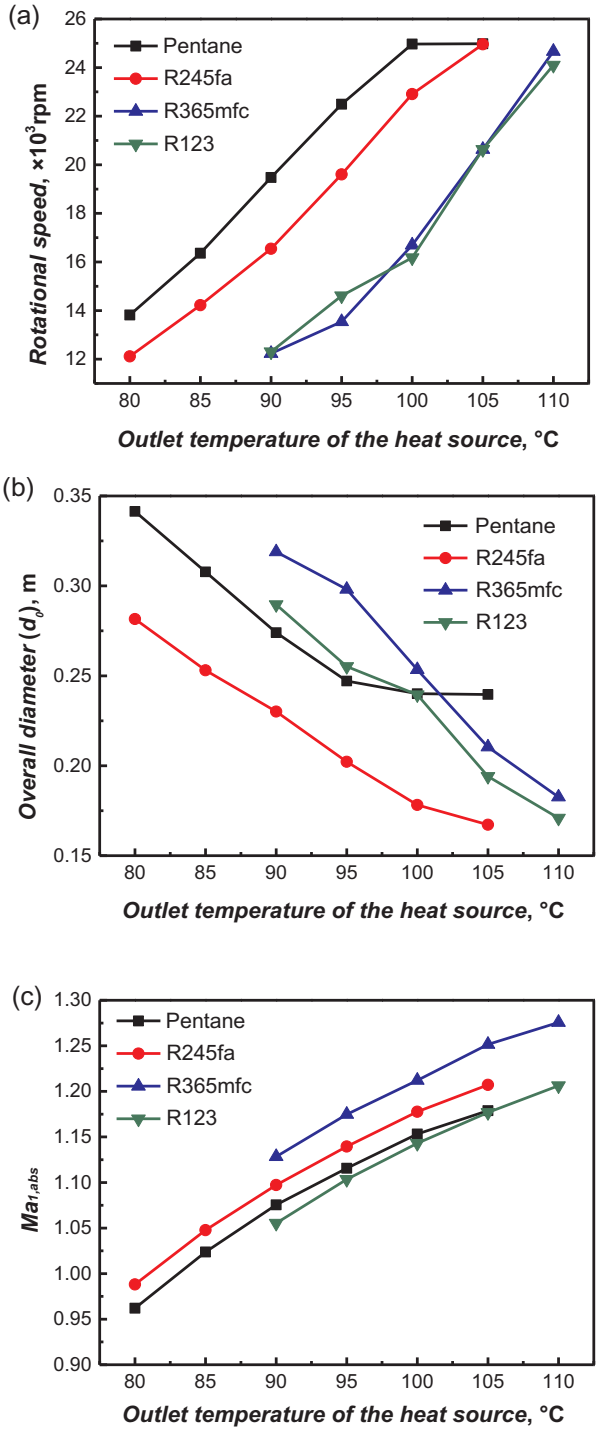

Fig. 13. Variation of rotational speed (a), overall diameter (b) and Mach number at the rotor inlet (c) with the outlet temperature of the heat source.

Table 6
Optimized results of the preliminary design for the examined working fluids at the maximum turbine efficiency condition.

Parameters	Pentane, 80 °C	R245fa, 80 °C	R365mfc, 90 °C	R123, 90 °C
d_0 (m)	0.3414	0.2816	0.3189	0.2896
$b_{1,n}$ (m)	0.0175	0.0135	0.0145	0.0138
$d_{1,n}$ (m)	0.2625	0.2166	0.2452	0.2227
d_1 (m)	0.2605	0.2146	0.2432	0.2207
b_1 (m)	0.0180	0.0139	0.0149	0.0142
b_1/d_1	0.0690	0.0646	0.0614	0.0643
$d_{2,s}$ (m)	0.2106	0.1730	0.1962	0.1782
$d_{2,h}$ (m)	0.0637	0.0498	0.0523	0.0553
Z_r	12	12	12	12
$Ma_{1,rel}$	0.2780	0.2868	0.3267	0.3065
$Ma_{1,abs}$	0.9621	0.9882	1.1284	1.0553
$Ma_{2,rel}$	0.5947	0.5987	0.6973	0.6618
$Ma_{2,abs}$	0.2481	0.2402	0.3054	1.0553
α_0 (deg.)	79.21	79.16	79.26	79.21
α_1 (deg.)	16.38	16.43	16.33	16.37
α_2 (deg.)	99.63	99.67	99.28	99.20
β_1 (deg.)	102.58	102.90	103.84	103.90
β_2 (deg.)	24.29	23.29	25.61	25.02
$\beta_{2,s}$ (deg.)	18.10	17.26	18.96	18.72
$\beta_{2,h}$ (deg.)	51.09	51.16	56.72	51.21
$d_{2,h}/d_1$	0.2445	0.2322	0.2151	0.2505
$\eta_{turbine}$ (%)	90.428	91.008	89.977	90.404

expansion at the rotor inlet, which is undesirable. It indicates that it is appropriate to use the TC-4P blade profile for nozzle since such kind of blade profile has lower loss in the transonic situation.

Based on the optimized results, the recommended ranges for the key six design parameters can be made: the degree of reaction is recommended as 0.5–0.51; the velocity ratio is recommended as 0.70–0.71; the loading coefficient is recommended as 0.88–0.93; the flow coefficient is recommended as 0.26–0.29; the ratio of wheel diameter is recommended as 0.51–0.6. Detailed results at the maximum turbine efficiency condition are shown in Table 6.

6. Conclusions

This paper proposes a coupled modeling of the ORC system and the radial-inflow turbine, which is designed by the mean-line approach with constrained GA to maximize the turbine efficiency. This model allows for the dynamic design of the ORC system and its radial-inflow turbine based on a wide range of operating conditions and a reasonable range of aerodynamic and geometric parameters. The influences of heat source outlet temperature on the performance of ORC and radial-inflow turbine are investigated for pentane, R245fa, R365mfc and R123. It is found that the turbine efficiency decreases as the outlet temperature of the heat source increases with the minimum efficiency of 88.06% and maximum efficiency of 91.01%. Moreover, the cycle efficiency increases monotonously with the increase of the heat source outlet temperature while the net power output has the opposite trend. The maximum turbine and cycle efficiencies of 91.01%, 12.18% are obtained by R245fa at the heat source outlet temperature of 80 °C and R123 at the heat source outlet temperature of 110 °C, respectively. In addition, the recommended ranges for the degree of reaction, velocity ratio, loading coefficient, flow coefficient and ratio of wheel diameter of radial-inflow turbine are 0.5–0.51, 0.70–0.71, 0.88–0.93, 0.26–0.29 and 0.51–0.6, respectively. The minimum overall diameter d_0 (=167.2 mm) is achieved by using R245fa at the heat source outlet temperature of 105 °C.

Compared with other coupled design for ORC and radial-inflow turbine, this study introduces the constrained GA into the preliminary design of radial-inflow turbine with the prediction models of the velocity coefficients of nozzle and rotor. This coupled model is dynamic with the aim of achieving the maximum turbine efficiency. This study highlights the potential and effectiveness of this coupled modeling in design analysis for the ORC system and its radial-inflow turbine. Further work will concentrate on the CFD simulation or experimental testing of an ORC radial-inflow turbine.

References

[1] Tchanche BF, Papadakis G, Lambrinos G, Frangoudakis A. Fluid selection for a low-temperature solar organic Rankine cycle. Appl Therm Eng 2009;29(11–12):2468–76.
[2] Delgadotorres AM, Garcíarodríguez L. Analysis and optimization of the low-temperature solar organic Rankine cycle (ORC). Energy Convers Manage 2010;51(12):2846–56.
[3] Besong OJ, Taccani R, Lucia MD, Micheli D, Toniato G. Development and experimental characterization of a small scale solar powered organic Rankine cycle (ORC). Associazione Termotecnica Italiana; 2016.
[4] Pantaleo AM, Ciliberti P, Camporeale S, Shah N. Thermo-economic assessment of small scale biomass CHP: steam turbines vs ORC in different energy demand segments. In: International conference on applied energy; 2015. p. 1609–17.
[5] Sansaniwal SK, Rosen MA, Tyagi SK. Global challenges in the sustainable development of biomass gasification: an overview. Renew Sustain Energy Rev 2017;80:23–43.
[6] Glover S, Douglas R, Rosa MD, Zhang X, Glover L. Simulation of a multiple heat source supercritical ORC (organic Rankine cycle) for vehicle waste heat recovery. Energy 2015;93:1568–80.
[7] Hettiarachchi HDM, Golubovic M, Worek WM, Ikegami Y. Optimum design criteria for an organic Rankine cycle using low-temperature geothermal heat sources. Energy 2007;32(9):1698–706.
[8] Cammarata G, Cammarata L, Petrone G. Thermodynamic analysis of ORC for energy production from geothermal resources. Energy Proc 2014;45:1337–43.
[9] Liu Q, Shen A, Duan Y. Parametric optimization and performance analyses of geothermal organic Rankine cycles using R600a/R601a mixtures as working fluids. Appl Energy 2015;148:410–20.
[10] Nemati A, Nam H, Ranjbar F, Yari M. A comparative thermodynamic analysis of ORC and Kalina cycles for waste heat recovery: a case study for CGAM cogeneration system. Case Stud. Therm. Eng. 2016;9:1–13.
[11] Yu G, Shu G, Tian H, Huo Y, Zhu W. Experimental investigations on a cascaded steam-/organic-Rankine-cycle (RC/ORC) system for waste heat recovery (WHR) from diesel engine. Energy Convers Manage 2016;129:43–51.
[12] Kim YM, Dong GS, Chang GK, Cho GB. Single-loop organic Rankine cycles for engine waste heat recovery using both low- and high-temperature heat sources. Energy 2016;96:482–94.
[13] Rahbar K, Mahmoud S, Aldadah R, Moazami N. Preliminary mean-line design and optimization of a radial turbo-expander for waste heat recovery using organic Rankine cycle. Energy Proc 2015;75(3):860–6.
[14] Srinivasan KK, Mago PJ, Zdaniuk GJ, Chamra LM, Midkiff KC. Improving the efficiency of the advanced injection low pilot ignited natural gas engine using organic Rankine cycles. J Energy Res Technol 2007;130(2):333–42.
[15] Erbas M, Biyikoglu A. Design and multi-objective optimization of organic Rankine turbine. Int J Hydrogen Energy 2015;40(44):15343–51.
[16] Wang EH, Zhang HG, Fan BY, Ouyangb MG, Zhaoc Y, Muc QH. Study of working fluid selection of organic Rankine cycle (ORC) for engine waste heat recovery. Energy 2011;36(5):3406–18.
[17] Rayegan R, Tao YX. A procedure to select working fluids for solar organic Rankine cycles (ORCs). Renew Energy 2011;36(2):659–70.
[18] Drescher U, Brüggemann D. Fluid selection for the organic Rankine cycle (ORC) in biomass power and heat plants. Appl Therm Eng 2007;27(1):223–8.
[19] Qiu G. Selection of working fluids for micro-CHP systems with ORC. Renew Energy 2012;48(6):565–70.
[20] Bao J, Zhao L. A review of working fluid and expander selections for organic Rankine cycle. Renew Sustain Energy Rev 2013;24(10):325–42.
[21] Peris B, Navarro-Esbrí J, Molés F, Collado R, Mota-Babiloni A. Performance evaluation of an organic Rankine cycle (ORC) for power applications from low grade heat sources. Appl Therm Eng 2014;75:763–9.
[22] Braimakis K, Karellas S. Integrated thermoeconomic optimization of standard and regenerative ORC for different heat source types and capacities. Energy 2017;121:570–98.
[23] Mehrpooya M, Ashouri M, Mohammadi A. Thermoeconomic analysis and optimization of a regenerative two-stage organic Rankine cycle coupled with liquefied natural gas and solar energy. Energy 2017;126:899–914.
[24] Yang MH, Yeh RH. Economic performances optimization of an organic Rankine cycle system with lower global warming potential working fluids in geothermal application. Renew Energy 2016;85:1201–13.
[25] Marion M, Voicu I, Tiffonnet AL. Study and optimization of a solar subcritical organic Rankine cycle. Renew Energy 2012;48(6):100–9.
[26] Wang JL, Zhao L, Wang XD. An experimental study on the recuperative low temperature solar Rankine cycle using R245fa. Appl Energy 2012;94(2):34–40.
[27] Xi H, Li MJ, He YL, Tao WQ. A graphical criterion for working fluid selection and thermodynamic system comparison in waste heat recovery. Appl Therm Eng 2015;89:772–82.
[28] Mago PJ, Chamra LM, Srinivasan K, Somayaji C. An examination of regenerative organic Rankine cycles using dry fluids. Appl Therm Eng 2008;28(8):998–1007.

[29] Vetter C, Wiemer HJ, Kuhn D. Comparison of sub- and supercritical organic Rankine cycles for power generation from low-temperature/low-enthalpy geothermal wells, considering specific net power output and efficiency. Appl Therm Eng 2013;51(1–2):871–9.
[30] Javanshir A, Sarunac N. Thermodynamic analysis of a simple organic Rankine cycle. Energy 2017;118:85–96.
[31] Dong BS, Xu GQ, Luo X, Zhuang LH, Quan YK. Analysis of the supercritical organic Rankine cycle and the radial turbine design for high temperature applications. Appl Therm Eng 2017;123:1523–30.
[32] Dong BS, Xu GQ, Cai Y, Li HW. Analysis of zeotropic mixtures used in high-temperature organic Rankine cycle. Energy Convers Manage 2014;84:253–60.
[33] Li Z, Bao J. Thermodynamic analysis of organic Rankine cycle using zeotropic mixtures. Appl Energy 2014;130(8):748–56.
[34] Fischer J. Comparison of trilateral cycles and organic Rankine cycles. Energy 2011;36(10):6208–19.
[35] Yari M, Mehr AS, Zare V, Mahmoudi SMS, Rosen MA. Exergoeconomic comparison of TLC (trilateral Rankine cycle), ORC (organic Rankine cycle) and Kalina cycle using a low grade heat source. Energy 2015;83:712–22.
[36] Fiaschi D, Manfrida G, Maraschiello F. Design and performance prediction of radial ORC turboexpanders. Appl Energy 2015;138(C):517–32.
[37] Song J, Gu CW, Ren X. Parametric design and off-design analysis of organic Rankine cycle (ORC) system. Energy Convers Manage 2016;112:157–65.
[38] Sauret E, Gu Y. Three-dimensional off-design numerical analysis of an organic Rankine cycle radial-inflow turbine. Appl Energy 2014;135(C):202–11.
[39] Kang SH. Design and preliminary tests of ORC (organic Rankine cycle) with two-stage radial turbine. Energy 2016;96:142–54.
[40] Jubori AA, Al-Dadah RK, Mahmoud S, Ennil ASB, Rahbar K. Three dimensional optimization of small-scale axial turbine for low temperature heat source driven organic Rankine cycle. Energy Convers Manage 2016;133:411–26.
[41] Song J, Gu CW, Ren X. Influence of the radial-inflow turbine efficiency prediction on the design and analysis of the organic Rankine cycle (ORC) system. Energy Convers Manage 2016;123:308–16.
[42] Pan L, Wang H. Improved analysis of organic Rankine cycle based on radial flow turbine. Appl Therm Eng 2013;61(2):606–15.
[43] Jubori AA, Daabo A, Al-Dadah RK, Mahmoud S, Ennil AB. Development of micro-scale axial and radial turbines for low-temperature heat source driven organic Rankine cycle. Energy Convers Manage 2016;130:141–55.
[44] Rahbar K, Mahmoud S, Al-Dadah RK, Moazami N. Modelling and optimization of organic Rankine cycle based on a small-scale radial inflow turbine. Energy Convers Manage 2015;91:186–98.
[45] Glassman AJ. Computer program for design analysis of radial-inflow turbines; 1976.
[46] Ji GH. Turbine expander. Beijing: Machinery Industry Press; 1989.
[47] Ventura CAM, Jacobs PA, Rowlands AS, Petrie-repar P, Sauret E. Preliminary design and performance estimation of radial inflow turbines: an automated approach.
[48] Jubori AMA, Al-Dadah RK, Mahmoud S, Daabo A. Modelling and parametric analysis of small-scale axial and radial-outflow turbines for organic Rankine cycle applications. Appl Energy 2017;190:981–96.
[49] Cauty R. Genetic algorithms and engineering optimization, genetic algorithms and engineering design. Wiley; 1997. p. 379–81.
[50] Lemmon E, Huber M, McLinden M. NIST standard reference database 23, NIST reference fluid thermodynamic and transport properties–REFPROP, version 9.0, standard reference data program, Gaithersburg (MD): National Institute of Standards and Technology; 2010.
[51] Concepts NREC. < http://www.conceptsnrec.com/ > ; 2012.
[52] Rahbar K, Mahmoud S, Al-Dadah RK, Moazami N. Parametric analysis and optimization of a small-scale radial turbine for organic Rankine cycle. Energy 2015;83:696–711.